# SELF-PROPELLED JUMPING CONDENSATE: FUNDAMENTAL MECHANISMS AND VAPOR-CHAMBER APPLICATIONS

**Fangjie Liu, Jonathan B. Boreyko,[§] Xiaopeng Qu and Chuan-Hua Chen***
[§]Now at Virginia Tech
*Author for correspondence
Department of Mechanical Engineering and Materials Science
Duke University
Durham, NC 27708-0300, USA
E-mail: chuanhua.chen@duke.edu

## ABSTRACT

On a superhydrophobic surface, condensate droplets can spontaneously jump perpendicularly to the surface upon coalescence. The self-propelled motion results from the surface energy released upon drop coalescence, while the out-of-plane jumping results from the superhydrophobic substrate breaking the symmetry of energy release. This paper summarizes our recent efforts to unfold the physical mechanisms of the self-propelled jumping with interfacial flow simulations, and to utilize the jumping condensate as a liquid return mechanism for vapor chambers. To investigate the mechanism of the self-propelled jumping, we report three-dimensional phase-field simulations of two identical spherical drops coalescing on a flat surface with a contact angle of 180°. The numerical simulations capture the spontaneous jumping process which follows the capillary-inertial scaling. Our simulations accurately predict the nearly constant jumping velocity of around 0.2 when scaled by the capillary-inertial velocity. We attribute this low nondimensional velocity to the substrate intercepting only a small fraction of the expanding liquid bridge. In closed-loop phase-change systems, self-propelled jumping drops on a superhydrophobic condenser offer a new mechanism to return the working fluid to the evaporator, eliminating the requirement for either external forces or wick structures along the return path. We report the heat transfer performance of a jumping-drop vapor chamber consisting of two parallel plates, a superhydrophobic condenser and a superhydrophilic evaporator. Such a design enables novel phase-change heat transfer systems such as planar thermal diodes and heat spreaders.

## INTRODUCTION

Vapor chambers offer passive yet effective phase-change heat transfer in a planar form factor useful for microelectronics cooling [1-5]. Conventional vapor chambers are essentially flat-plate heat pipes [1-3], relying on wicked or grooved walls to return the working fluid from the condenser back to the evaporator by capillarity. For the capillary return to be effective, porous wick structures or fine grooves are required along the entire return path which poses design constraints and manufacturing complexities; see for example [6-9]. Alternative mechanisms such as gravitational and electrohydrodynamic return have their own limitations, rendering the heat transfer devices dependent on orientation or active power input [3]. Planar heat spreaders can also be obtained by arranging one-dimensional pipes such as thermosyphons and pulsating heat pipes into a plate [1,2], but such arrangements are less versatile because of the inherent one-dimensional tubular design, and are not effective for certain applications such as planar thermal diodes [10].

Here, we introduce a novel jumping-drop mechanism for condensate return, enabling an inherently planar vapor chamber and circumventing the drawbacks of gravity- or capillarity-driven return mechanisms. Rather than lining the entire vapor chamber with a wick structure, a wickless superhydrophobic plate was placed parallel to a wicked superhydrophilic plate, such that water condensing on the superhydrophobic surface would spontaneously jump across the gap directly back to the wicked evaporator (Figure 1a). The kinetic energy required for the jumping-drop phenomenon is harvested from the surface energy released upon coalescence, and the out-of-plane directionality is a result of the superhydrophobic surface breaking the symmetry of energy release [11-18].

Our jumping-drop chamber builds upon conventional vapor chambers with a few notable differences owing to the new liquid return mechanism. (i) The superhydrophilic evaporator design is directly borrowed from wicked vapor chambers, with the same capillary redistribution mechanism of the working fluid within the wick structures; however, the mass flow rate is no longer dictated by the cross sectional area of the wick (i.e. proportional to the thickness of the wick), but by the frequency and size distribution of the jumping condensate drops. The jumping return therefore circumvents the capillary wicking limit, which is typically the most significant limit of moderate temperature heat

pipes and vapor chambers [1]. (ii) The perpendicular jumping return path between the condenser and the evaporator resembles the directionality of gravity-driven return in themosyphons; however, the jumping drops are much smaller and faster and therefore independent of gravitational orientation [12]. The out-of-plane jumping return is scalable and particularly suitable for planar systems, unlike conventional vapor chambers with capillary return along wicked walls, where longer liquid return paths are expected for devices of larger areas. (iii) The jumping-drop vapor chamber consisting of condensers and evaporators of asymmetric wettability is a thermal diode by design [10], in contrast to conventional wicked vapor chambers with symmetric (interchangeable) condenser and evaporator.

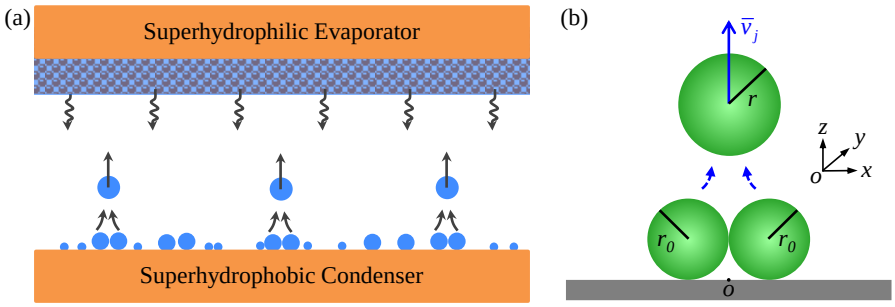


**Figure 1**. (a) Schematic of the jumping-drop vapor chamber consisting of a superhydrophobic evaporator and a superhydrophilic condenser in parallel. Heat is removed by evaporation of liquid water contained in the wicked evaporator, and rejected at the condenser by condensation of the water vapor. The working fluid is returned back to the evaporator by the self-propelled jumping phenomenon, where condensate drops spontaneously jump out-of-plane upon drop coalescence on the superhydrophobic surface. (b) Schematic of the drop coalescence process on a non-wetting substrate. Two adjacent drops with an initial radius $r_0$ coalesce into a larger spherical drop with an equilibrium radius of $r = 2^{1/3} r_0$. The reduction in surface area releases excess surface energy, powering the merged drop to jump away from the substrate.

The jumping process is known to be governed by the capillary-inertial scaling laws [11,12], which can be understood from the energetic point of view (Figure 1b). When two identical drops of radius $r_0$ coalesce into a larger one, the equilibrium radius is $r=2^{1/3} r_0$ for the merged drop with a mass of $m = \frac{8}{3}\rho_L \pi r_0^3$, where $\rho_L$ is the density of the liquid. The overall surface area is reduced upon coalescence, leading to the release of surface energy in the amount of $\Delta E_s = 4\sigma\pi r_0^2 (2 - 2^{2/3})$, where $\sigma$ is surface tension of the air-liquid interface. The presence of the substrate breaks the symmetry of energy release and the merged drop eventually jumps up. The symmetric coalescence of two identical drops leads to a vertical jumping velocity ($\bar{v}_j$), which is expected to follow the capillary-inertial scaling,

$$\bar{v}_j \sim u_{ci} = \sqrt{\frac{\sigma}{\rho_L r_0}}, \tag{1}$$

where $u_{ci}$ is the capillary-inertial velocity. In fact, if all the released surface energy were converted to kinetic energy, the merged drop could achieve a jumping velocity of $\sqrt{2\Delta E_s / m} = 1.11 u_{ci}$. The $r_0^{-1/2}$ scaling in Equation (1) has indeed been confirmed by the experiments with coalescing drops of water condensate on textured superhydrophobic surfaces; However, the jumping velocity of the merged drop is significantly smaller than the capillary-inertial velocity with $\bar{v}_j \approx 0.2 u_{ci}$. In terms of the energy conversion efficiency, the kinetic energy associated with the jumping motion is less than 4% of the total released surface energy ($\frac{1}{2} m \bar{v}^2 \lesssim 4\% \Delta E_s$). The low nondimensional jumping velocity is a puzzle of practical significance, e.g. for designing vapor chambers with orientation-independent jumping condensate.

This paper summarizes our recent efforts to unfold the physical mechanisms of the self-propelled jumping with interfacial flow simulations [19], and to utilize the jumping condensate as a liquid return mechanism for vapor chambers [20]. We will first present a physical model for the self-propelled jumping with phase-field numerical solutions. The physical insights from the numerical simulations will then be used to resolve the aforementioned puzzle on the jumping velocity. We will then discuss the novel vapor chamber and focus on the unique aspects due to the jumping return mechanism. The inherently planar design justifies the simplification of the system as serial resistances due to wick conduction and interfacial phase change. The capability of the jumping drops to travel against gravity presents new operating limits to our vapor chamber. The directional jumping gives rise to thermal rectification.

## MECHANISMS OF SELF-PROPELLED JUMPING

As sketched in Figure 1b, our physical model consists of two static drops coalescing on a perfectly flat substrate with a contact angle of 180°. Gravity is neglected since the radii of the jumping drops of interest here are much smaller than the capillary length. Building upon the work of Feng and coworkers [21,22], we have implemented a three-dimensional (3D) numerical simulation using the phase-field method to capture the evolution of air-liquid interfaces with rapidly changing topology; see [19] for details. In Figure 2a, the coalescence-induced jumping process is simulated. At $t^* = 0$, the coalescence is initiated by the overlapping of diffuse interfaces. A liquid bridge forms upon coalescence and the expanding bridge reaches the substrate around 0.88, at which point the merged drop starts to experience an upward net movement. The substrate counteracts the impingement of the liquid bridge, forcing a portion of the downward-moving mass toward the sides, leading to a maximum deformation in the x-direction at 1.14. The upward force from the substrate peaks at 1.88, beyond which the apparent contact area between the merged drop and the substrate gradually reduces toward zero at 2.58, the point of departure. The launched drop continues to oscillate while maintaining the upward motion. In Figure 2b, the substrate is removed and the coalescence occurs in the air, and the merged drop merely experiences free oscillation.

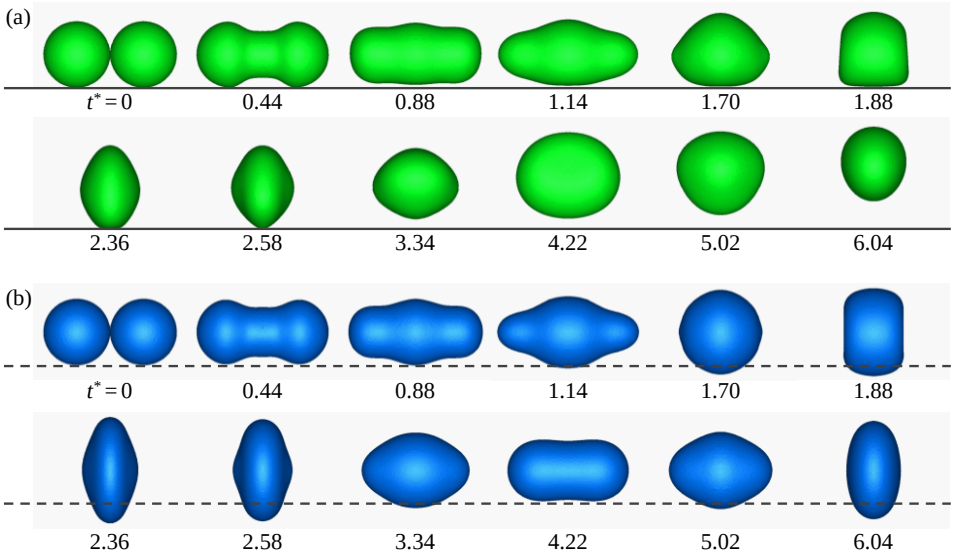


**Figure 2**. The 3D coalescence process of two static drops: (a) Side xz-view for coalescence-induced jumping on a flat substrate with a contact angle of 180°, with the substrate represented by the solid line. (b) Side xz-view of the corresponding coalescence process in the air, where the center of mass is relocated to the center of the computational domain. The dashed line is a visual guide for an imaginary substrate in the side view. The capillary-inertial time scale, $\tau_{ci} = \sqrt{\rho_L r_0^3 / \sigma}$, is used to nondimensionalize time.

The jumping motion is a consequence of the interaction between the oscillation of the merged drop and the non-wetting substrate. To understand the jumping mechanism, it is helpful to first review drop coalescence in the air. Without any interaction with the substrate, two initially distinct drops will merge by the formation of a liquid bridge. Following the expansion of the liquid bridge, the merged drop will oscillate between oblate and prolate shapes, eventually relaxing by viscous action to a larger spherical drop. In the absence of the substrate, top-down symmetry is preserved throughout the oscillation process. Note that part of the oscillating drop crosses the imaginary substrate represented by a dashed line, which must be the case because the radius of the merged drop is larger than that of the initial drops. When a non-wetting substrate is present, the impermeable wall will force the fraction of the mass that would have crossed the dashed line to move upward, leading to the jumping motion.

Since the kinetic energy for the self-propelled jumping is converted from the surface energy released upon coalescence, additional insights can be gained by directly tracking the energy conversion process. In Figure 3, the surface and kinetic energies of the merged drop are calculated by integration over the entire computational domain. Akin to the König theorem for the kinetic energy of many bodies, the kinetic energy of an isolated drop can be further decomposed by noting

$$\int_\Omega \mathbf{v}\cdot\mathbf{v} d\Omega = \int_\Omega \bar{\mathbf{v}}\cdot\bar{\mathbf{v}} d\Omega + \int_\Omega \hat{\mathbf{v}}\cdot\hat{\mathbf{v}} d\Omega, \tag{2}$$

where $\bar{\mathbf{v}}$ is the average velocity of the drop and $\hat{\mathbf{v}} = \mathbf{v} - \bar{\mathbf{v}}$ is the velocity with respect to the center of mass. In the absence of any rotational motion, the kinetic energy is attributed to either translational or oscillatory motion, $E_k = E_{k,tr} + E_{k,os}$. As far as the self-propelled jumping is concerned, the translational kinetic energy associated with $\bar{v}$ is the only useful part, which arises from the substrate breaking the top-down symmetry of the coalescence-induced motion. For drop coalescence in the air, the ensuing motion is completely oscillatory. Aside from the viscous dissipation, the overall surface energy exchanges with the total kinetic energy during the capillary-inertial oscillation, evident by their anti-phase variations over time. Since the translational kinetic energy ( $E_{k,tr}$ ) is only a small fraction of the total kinetic energy and is more or less constant after departure (Figure 3b), the energy exchange is mostly between the surface energy and the oscillatory kinetic energy ( $E_{k,os}$ ).

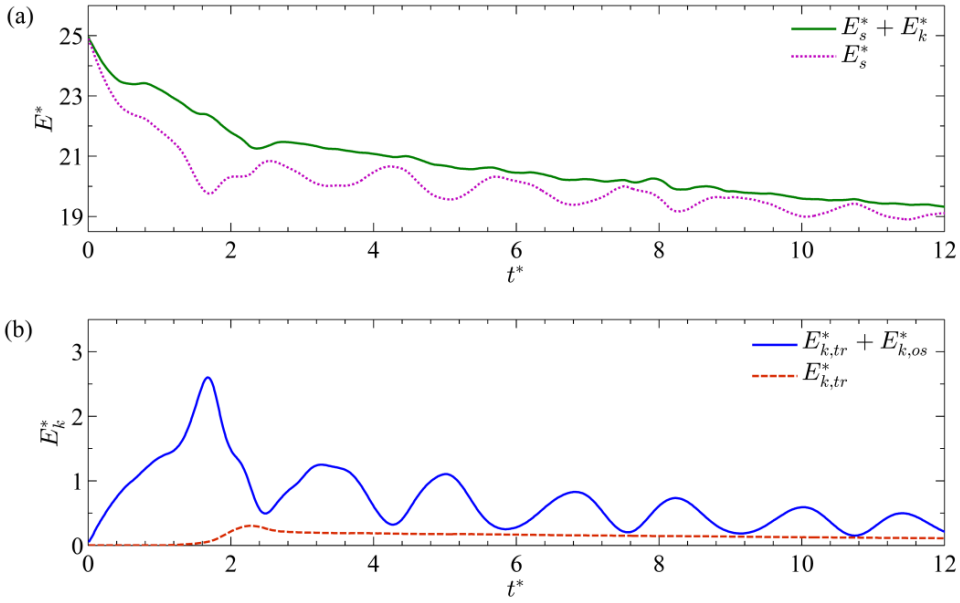


**Figure 3**. Surface and kinetic energy ( $E_s$ and $E_k$ ) of the merged drop during the jumping process of Figure 2a. The energies are non-dimensionalized by $\sigma r_0^2$. (a) The combination of surface and kinetic energy decays over time because of viscous dissipation. The damped oscillation of energy has an approximate period of $\pi/2$. (b) The kinetic energy of the merged drop can be decomposed into translational and oscillatory components. The oscillatory component does not contribute to any net motion and will be dissipated eventually.

The nondimensional jumping velocity of $\bar{v}_j^* \approx 0.2$ in the capillary-inertial regime can be rationalized by the following heuristic argument (Figure 4). Based on the numerical solution of the control case without the substrate, a maximum of 9.4% of the total mass ( $m$ ) crosses the imaginary substrate represented by the dashed line when the merged drop extends to the maximum prolate configuration, i.e. $\Delta m_d \approx 10\% m$ in Figure 4b. The presence of the substrate forces a lumped mass of $\Delta m_d$ that initially moves downward at approximately $u_{ci}$ to eventually "bounce" upward, in a manner analogous to the elastic rebound of entire drops on superhydrophobic surfaces. At the same time, the "unbalanced" counter mass of $\Delta m_d$ on top of the merged drop continues to move upward at approximately $u_{ci}$ [19]. As a result of the substrate breaking the symmetry of the surface energy release, two chunks of liquid, each with a mass of $\Delta m_d$, are forced by the substrate to move upward at the capillary-inertial velocity, while the rest of drop still maintains the approximate top-down symmetry. Effectively, the non-wetting substrate provides a vertical impulse $J_z \sim 2\Delta m_d u_{ci}$. When the vertical momentum is distributed over the total drop mass, the mass-averaged jumping velocity can be approximated as

$$\bar{v}_j \sim \frac{J_z}{m} \sim \frac{2\Delta m_d}{m} u_{ci}. \tag{3}$$

Accordingly, the nondimensional velocity is approximated by $\bar{v}_j^* \sim 2\Delta m_d / m \approx 0.2$.

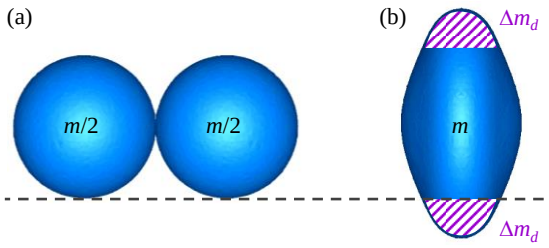


**Figure 4**. The symmetry-breaking action of the substrate can be estimated by the drop coalescence cases in the air: (a) Coalescence of two static drops of initial radius $r_0$, each with a mass of $m/2$. (b) For the maximum capillary-inertial deformation of the merged drop ($t^*$=2.36 in Figure 2b), the dynamic crossing mass that passes below the imaginary substrate is $\Delta m_d = 9.4\% m$.

For the self-propelled jumping on non-wetting substrates, the energy conversion efficiency is low when the useful translational kinetic energy ($E_{k,tr}$) is compared to the released surface energy ($\Delta E_s$). The low efficiency is directly related to the small nondimensional jumping velocity, since $E_{k,tr}/\Delta E_s \approx \bar{v}_j^{*2}$. Most of the released surface energy is viscously dissipated, including the majority of the energy that is first stored in the oscillatory motion (Figure 3b). The mechanistic insight to the direction and magnitude of the jumping velocity is useful below in modeling the jumping-condensate vapor chamber.

## VAPOR CHAMBERS WITH JUMPING CONDENSATE

In Figure 1a, the jumping-drop vapor chamber consists of two parallel plates enclosing water in both liquid and vapor phases. The working fluid is circulated as follows: the liquid water evaporates from the wick structure embedded on the superhydrophilic evaporator, the water vapor condenses on the opposing superhydrophobic condenser, and the condensate jumps back to the evaporator upon drop coalescence. The parallel-plate configuration justifies the following one-dimensional model for the effective heat transfer coefficient and the gravitational limit of operation specific to the jumping return. The overall heat transfer coefficient of the jumping-drop vapor chamber ($h_o$) is dependent on the conduction resistance across the wick which is almost independent of temperature, and the interfacial resistances across the evaporator and condenser which strongly depend on the vapor temperature,

$$\frac{1}{h_o} \approx \frac{H_w}{k_w} + \frac{1}{h_i} + \frac{1}{\hat{\chi} h_i} \equiv \frac{H_w}{k_w} + \frac{1}{h_{pc}}, \tag{4}$$

where $H_w$ is the thickness of the wick structure, $k_w$ is the effective conductivity of the water-saturated wick, $h_i$ is the interfacial heat transfer coefficient. The geometrical parameter $\hat{\chi}$ accounts for the partial coverage of dropwise condensate on the condenser surface and also the fact that the actual surface area of a drop open to additional condensation is larger than its projected area on the condenser. The lumped heat transfer coefficient ($h_{pc}$) due to phase change on both the evaporator and the condenser is given by,

$$h_{pc} \approx \frac{\hat{\chi}}{1+\hat{\chi}} h_i \approx \hat{\beta} \frac{\rho_v h_{lv}^2}{T_v} \sqrt{\frac{\bar{M}}{2\pi \bar{R} T_v}}, \tag{5}$$

where $\hat{\beta}$ absorbs both $\hat{\chi}$ and the accommodation coefficient $\hat{\alpha}$ in $h_i$, $\rho_v$, $h_{lv}$, and $\bar{M}$ are the density, latent heat, and molecular weight of the saturated water vapor at a temperature $T_v$, and $\bar{R}$ is the universal gas constant. [23,24].

For orientation independence with the new return mechanism, the jumping drops must be able to travel against gravity to reach the counter plate. The gravitational limit is reached when the separation between the condenser and evaporator plates (i.e. the vapor spacing $H_v$) exceeds a critical value, such that the jumping condensate cannot consistently return to the evaporator, leading to dryout in the orientation with the drops jumping "against gravity". The maximum jumping height against gravity is therefore given by,

$$H_v^G \sim \frac{\bar{v}_j^2}{2g}, \tag{6}$$

where $g$ is the gravitational acceleration.

A vapor chamber is assembled according to the schematic in Figure 1a with a superhydrophilic wick plate and a superhydrophobic condenser plate; see [20] for detailed experimental procedures. According to the simplified model in Equation (4), the overall thermal resistance mainly consists of the conduction resistance through the thickness of the wick and the phase-change interfacial resistances. To test this model, the thickness of the wick is varied while its thermal conductivity is kept constant (Figure 5). The results indicate better heat transfer performance at smaller wick thickness, confirming the importance of the conduction resistance across the wick. When the lumped phase-change heat transfer coefficient is deduced from experimental measurements as $1/h_{pc} = 1/h_o - H_w/k_w$, a nearly exponential dependence of $h_{pc}$ on the vapor temperature ($T_v$) is observed, consistent with Equation (5).

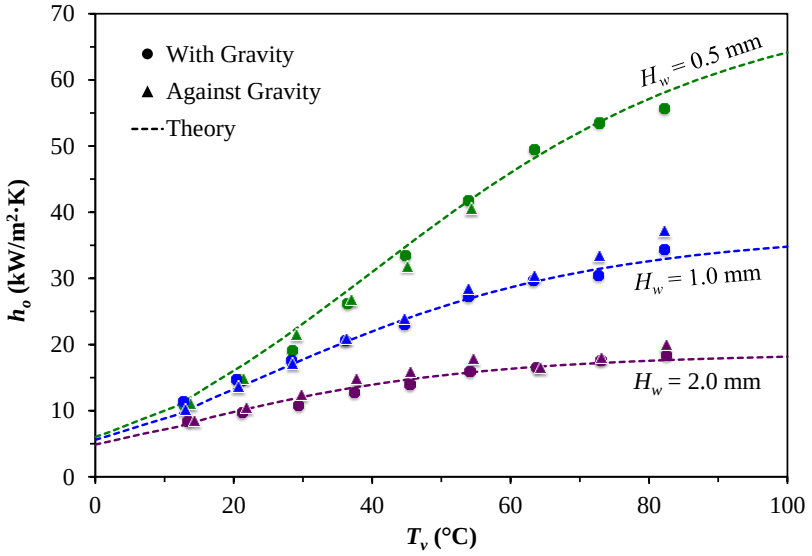


**Figure 5**. The overall heat transfer coefficient ($h_o$) as a function of the vapor temperature ($T_v$), where the wick thicknesses is $H_w$ = 0.5 mm, 1.0 mm, and 2.0 mm. The vapor chamber performance is orientation independent, except for the $H_w$ = 0.5 mm wick at high vapor temperatures where the corresponding vapor spacing is $H_v$ = 2.0 mm. The dashed lines are based on the lumped resistance model in Equations (4) and (5) with only one fitting parameter, $\hat{\beta}$, which is set as 0.053.

The performance in Figure 5 agrees well with Equation (4) with $\hat{\beta}$ = 0.053, which represents the reasonable combination of a geometrical parameter of $\hat{\chi} = 1$ [20] and an accommodation coefficient of $\hat{\alpha} \approx 0.1$, which is around the maximum attainable for "stagnant interfaces" [24]. At low vapor temperatures ($T_v$), the overall thermal resistance ($1/h_o$) is dominated by the phase-change resistances ($1/h_{pc}$) which decreases exponentially with $T_v$. At higher temperatures, the vapor chamber is dominated by the wick resistance ($H_w/k_w$) which is nearly independent of $T_v$ but strongly depends on the wick thickness ($H_w$).

To investigate the gravitational dependence, the vapor spacing is varied by changing the gasket thickness between the condenser and evaporator plates, and the resulting vapor chamber is tested with the drops jumping "with gravity" and "against gravity" (Figure 6). With the wick thickness fixed at $H_w$ = 1.0 mm, the vapor spacing is varied with $H_v$ = 0.8, 1.5, and 2.7 mm. In the "with gravity" orientation, the overall heat transfer coefficient is equivalent for all three vapor spacings, consistent with the independence to $H_v$ implied in Equation (4). In the "against gravity" orientation, however, dryout occurs consistently with $H_v$ = 2.7 mm, indicating that a large portion of the condensate drops cannot jump back to the evaporator. Although the threshold vapor spacing for the gravitational dependence is difficult to pinpoint, it should be around 2.0 mm based on tests plotted in Figure 5. According to Equation (6), the gravitational limit of $H_v^G \approx$ 2.0 mm corresponds to a condensate drop velocity of $u_l \sim$ 0.2 m/s. From this estimate of the jumping velocity, the average diameter of the jumping drops is of order $R_l \sim$ 100 μm based on Equation (1) noting that $\bar{v}_j^* \approx 0.2$. These estimates are consistent with our earlier measurements, albeit in open air [12].

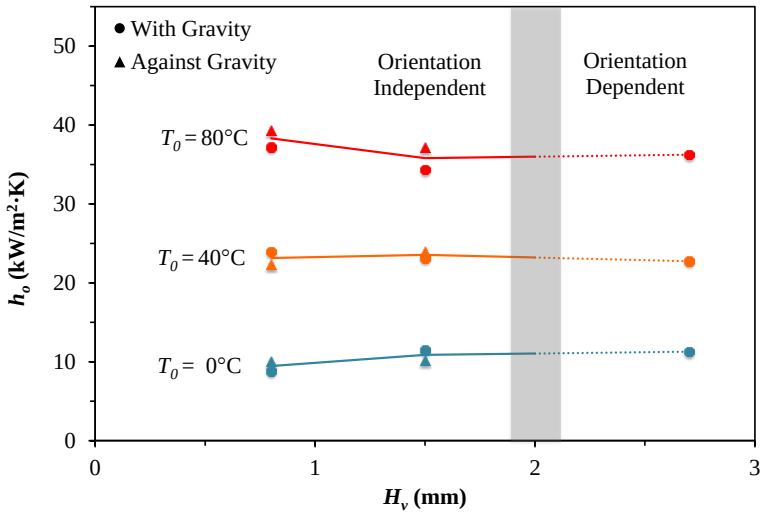


**Figure 6**. The overall heat transfer coefficient ($h_o$) as a function of the vapor spacing ($H_v$). For relatively small vapor spacing, $h_o$ is essentially independent of $H_v$ regardless of the orientation. Above a critical limit of $H_v^m \approx$ 2.0 mm, however, dryout occurs in the "against gravity" orientation.

The jumping-drop vapor chamber consisting of two parallel plates with asymmetric wettability can be exploited for thermal rectification [10]. In Figure 5, we have shown that a heat flux imposed on the superhydrophilic surface can be effectively removed via phase-change heat transfer (the forward mode). If the direction of the heat flow is reversed and the superhydrophobic surface is heated instead, no latent heat transfer is expected (the reverse mode). The thermal rectification by the jumping-drop vapor chamber is well conveyed by the following comparison in Figure 7. In the forward mode with a temperature difference of 2.0°C, a heat flux of 8.1 W/cm$^2$ is transported from the hotter superhydrophilic surface to the colder superhydrophobic one; In the reverse mode with the same temperature difference, only 0.033 W/cm$^2$ is transported in the opposite direction. This ratio of forward and reverse heat flux under otherwise identical conditions yields a rectification coefficient (diodicity) of approximately 250.

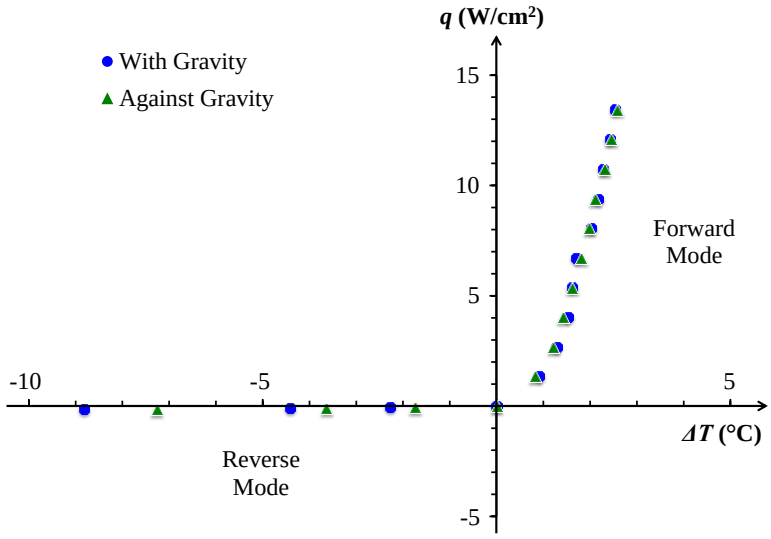


**Figure 7**. The jumping-drop chamber is inherently a thermal diode, transporting heat effectively only when the superhydrophilic surface is hotter than the superhydrophobic one, i.e. in the forward mode with $\Delta T > 0$.

## CONCLUSIONS

Based on drop coalescence processes with and without the substrate, the out-of-plane jumping results from the non-wetting substrate interfering with the oscillation of the merged drop. The small nondimensional jumping velocity of approximately 0.2 is attributed to the substrate only intercepting a small fraction of the oscillating drop.

Consequently, only a tiny fraction of the released surface energy is converted into the translational kinetic energy for the upward motion, the rest being stored in oscillatory modes and eventually dissipated.

Taken advantage of both the spontaneity and directionality of the jumping drops, we have developed a novel vapor chamber that recirculates the working fluid via the jumping mechanism. The overall heat transfer coefficient of the degassed vapor chamber is dominated by the interfacial phase-change resistances at low vapor temperatures and the wick conduction resistance at high vapor temperatures. The jumping return mechanism restricts the chamber performance with a gravitational limit. The jumping-drop vapor chamber is inherently a thermal diode.

## REFERENCES


[1] G. P. Peterson, *An Introduction to Heat Pipes: Modeling, Testing, and Applications*, Wiley-Interscience, New York, 1994.

[2] A. Faghri, *Heat Pipe Science and Technology*, Taylor & Francis, New York, 1995.

[3] D. Reay, P. Kew, *Heat Pipes*, 5th Edition, Butterworth-Heinemann, Oxford, 2006.

[4] I. Sauciuc, G. Chrysler, R. Mahajan, R. Prasher, Spreading in the heat sink base: Phase change systems or solid metals?, *IEEE Trans. Compon. Pack. Tech.* 25 (2002) 621–628.

[5] R. Mahajan, C. P. Chiu, G. Chrysler, Cooling a microprocessor chip, *Proc. IEEE* 94 (2006) 1476–1486.

[6] D. A. Benson, R. T. Mitchell, M. R. Tuck, D. W. Palmer, G. P. Peterson, Ultrahigh-capacity micromachined heat spreaders, *Microscale Therm. Eng.* 2 (1998) 21–30.

[7] R. Hopkins, A. Faghri, D. Khrustalev, Flat miniature heat pipes with micro capillary grooves, *J. Heat Transfer* 121 (1999) 102–109.

[8] Y. Wang, K. Vafai, An experimental investigation of the thermal performance of an asymmetrical flat plate heat pipe, *Int. J. Heat Mass Transfer* 43 (2000) 2657–2668.

[9] S. Kalahasti, Y. K. Joshi, Performance characterization of a novel flat plate micro heat pipe spreader, *IEEE Trans. Compon. Pack. Tech.* 25 (2002) 554–560.

[10] J. B. Boreyko, Y. Zhao, C. H. Chen, Planar jumping-drop thermal diodes, *Appl. Phys. Lett.* 99 (2011) 234105.

[11] M. Kollera, U. Grigull, Über das abspringen von tropfen bei der kondensation von quecksilber (The bouncing off phenomenon of droplets with condensation of mercury), *Heat Mass Transfer*, 2 (1969) 31–35.

[12] J. B. Boreyko, C. H. Chen, Self-propelled dropwise condensate on superhydrophobic surfaces, *Phys. Rev. Lett.* 103 (2009) 184501.

[13] C. Dietz, K. Rykaczewski, A. G. Fedorov, Y. Joshi, Visualization of droplet departure on a superhydrophobic surface and implications to heat transfer enhancement during dropwise condensation, *Appl. Phys. Lett.* 97 (2010) 033104.

[14] K. Rykaczewski, J. H. J. Scott, S. Rajauria, J. Chinn, A. M. Chinn, W. Jones, Three dimensional aspects of droplet coalescence during dropwise condensation on superhydrophobic surfaces, *Soft Matt.* 7 (2011) 8749–8752.

[15] X. Chen, J. Wu, R. Ma, M. Hua, N. Koratkar, S. Yao, Z. Wang, Nanograssed micropyramidal architectures for continuous dropwise condensation, *Adv. Funct. Mater.* (2011) 4617–4623.

[16] R. Enright, N. Miljkovic, A. Al-Obeidi, C. V. Thompson, E. N. Wang, Condensation on superhydrophobic surfaces: The role of local energy barriers and structure length scale, *Langmuir* 28 (2012) 14424–14432.

[17] M. He, X. Zhou, X. Zeng, D. Cui, Q. Zhang, J. Chen, H. Li, J. Wang, Z. Cao, Y. Song, L. Jiang, Hierarchically structured porous aluminum surfaces for high-efficient removal of condensed water, *Soft Matt.* 8 (2012) 2680–2683.

[18] N. Miljkovic, R. Enright, Y. Nam, K. Lopez, N. Dou, J. Sack, E. N. Wang, Jumping-droplet-enhanced condensation on scalable superhydrophobic nanostructured surfaces, *Nano Lett.* 13 (2013) 179–187.

[19] F. Liu, G. Ghigliotti, J. J. Feng, C. H. Chen, Numerical simulations of self-propelled jumping upon drop coalescence on non-wetting surfaces, *J. Fluid Mech.* 752 (2014) 39–65.

[20] J. B. Boreyko and C. H. Chen, Vapor chambers with jumping-drop liquid return from superhydrophobic condensers, *Int. J. Heat Mass Transfer* 61 (2013) 409–418.

[21] P. Yue, C. Zhou, and J. J. Feng, A computational study of the coalescence between a drop and an interface in Newtonian and viscoelastic fluids, *Phys. Fluids* 18 (2006) 102102.

[22] C. Zhou, P. Yue, J. J. Feng, C. F. Ollivier-Gooch, H. H. Hu, 3D phase-field simulations of interfacial dynamics in Newtonian and viscoelastic fluids, *J. Comput. Phys.* 229 (2010) 498–511.

[23] V. Carey, *Liquid-Vapor Phase-Change Phenomena*, 2nd Edition, Taylor & Francis, New York, 2008.

[24] R. Marek, J. Straub, Analysis of the evaporation coefficient and the condensation coefficient of water, *Int. J. Heat Mass Transfer* 44 (2001) 39–53.